Materials Science Forum Vols. 790-791 (2014) pp 396-401

doi:10.4028/www.scientific.net/MSF.790-791.396

Influence of Crystal Morphological Parameters on the Solidification of ESR Ingot

E. Karimi-Sibaki[1,a], A. Kharicha[1,2,b], J. Korp[3,c], M. Wu[1,2,d] and A. Ludwig[2,e]

[1] Christian Doppler Laboratory for Advanced Process Simulation of Solidification and Melting,

[2] Chair of Simulation and Modeling of Metallurgical Processes, Univ. of Leoben, Austria

[3] Schmiedetechnik Breitenfeld GmbH, 8662 Mitterdorf im Mürztal, Austria

[a] ebrahim.karimi-sibaki@unileoben.ac.at, [b] abdellah.kharicha@unileoben.ac.at,

[c] Joerg.korp@breitenfeld.at, [d] menghuai.wu@unileoben.ac.at, [e] ludwig@unileoben.ac.at

Keywords: Electroslag remelting, AC frequency, Dendrite arm spacing, Permeability.

Abstract. Electroslag remelting (ESR) is an advanced process to produce high quality steel. During the ESR process, the steel electrode is melted and then solidified directionally in a water-cooled mold. The quality of the ingot is strongly dependent on the shape of melt pool, i.e. the depth and thickness of mushy zone, which is in turn influenced by the bulk and interdendritic flow. Here, we perform a numerical study to investigate the effect of crystal morphological parameter such as primary dendrite arm spacing on the solidification of the ESR ingot (ϕ 750 mm). The crystal morphology is dominantly columnar and dendritic, thus a mixture enthalpy-based solidification model is used. Accordingly the mushy zone is considered as a porous media where the interdendritic flow is calculated based on the permeability. The permeability is determined as function of the liquid fraction and primary dendrite arm spacing according to Heinrich and Poirier [Comptes Rendus Mecanique, 2004, pp. 429-445]. The modeling results were verified against experimental results.

Introduction

Electroslag remelting (ESR) process is known for production of homogenous ingot with minimal defects such as macrosegregation, accumulation of non-metallic inclusions, and microporosity [1]. Within the process, the melt pool is solidified directionally that results in uniform and relatively fine dendritic structure [2]. The dendritic structure is mostly influenced by the cooling rate in the process, temperature gradient ahead of the crystallization front, and the intensity of interdendritic flow. With the increase of cooling rate, the local solidification time decreases and the mushy zone becomes thinner. Furthermore, an intensive flow in the melt pool promotes the formation of the freckles and leads to macrosegregation [3]. Slow and laminar interdendritic flow is desirable to achieve a finer structure for the final ingot. Principally, the flow is driven by the induced magnetic field that strongly depends on the operating conditions of the process. Over the last decades, attempts have been made to predict the melt pool shape of an ESR ingot using CFD models [4-6]. Most often, the decay of liquid movement in mushy zone has been modeled using the isotropic drag law of Carman-Kozeny [7] in which the dependency of permeability on the direction of solidification is ignored. In the meanwhile, some efforts were done to calculate the dendrite arm space based on local solidification time for ESR process [8-9]. In the current study, the effect of the direction of solidification on the interdendritic flow is considered using an anisotropic model for permeability. For this purpose, the distribution of dendrite arm space is calculated for the ESR ingot. Then, the effect of local variation in arm space on the directional permeability is taken into account. Additionally, the importance of dendrite arm space on the predicted melt pool shape is investigated by performing another simulation in which the parameter is kept homogenously constant in the mushy zone. The goal is to achieve some fundamental understanding of the formation of melt pool of solidifying ESR ingot considering the influence of crystal morphology and interdendritic velocity.

The Numerical model

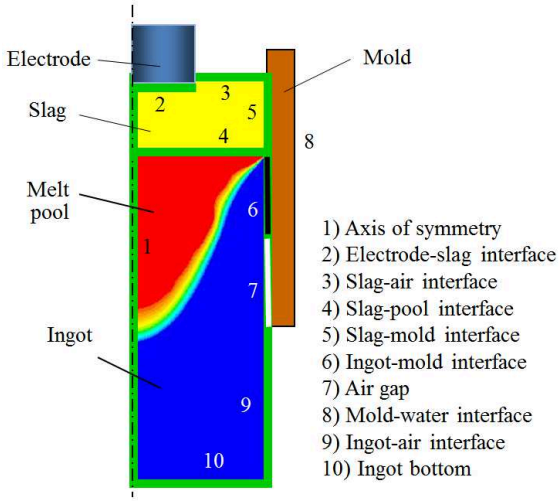

Fig. 1. Schematic representation of the computational domain and boundaries.

The Finite Volume Method (FVM) is applied to simulate the fluid flow, electromagnetic field, heat transfer and solidification during the ESR process. The required modeling equations are implemented in the commercial CFD software, FLUENT-ANSYS v.14.5, using User-Defined Functions (UDF). The computational domain and boundaries are schematically illustrated in Fig. 1. The induced magnetic field has only azimuthal direction, and thus the conditions are axisymmetric in the process. The latter is expressed using the phasor notation ($B_\theta = \widetilde{B}_\theta e^{i\Omega t}$) in which Ω is the angular frequency.

After computing the magnetic field (Eq. 1), the electric current ($\widetilde{\vec{j}}$) can be obtained through Ampere's law (Eq. 2):

$$\frac{\partial B_\theta}{\partial t} + \left[\frac{\partial}{\partial z}\left(\frac{1}{\sigma\mu_0}\frac{\partial B_\theta}{\partial z}\right) + \frac{\partial}{\partial r}\left(\frac{1}{r\sigma\mu_0}\frac{\partial (rB_\theta)}{\partial r}\right)\right] = 0. \tag{1}$$

$$\widetilde{\vec{j}} = \frac{1}{\mu_0}(\vec{\nabla}\times\widetilde{B}_\theta)\cdot \tag{2}$$

Finally, the Lorentz force ($\vec{F}_L$) and Joule heating (Q) are computed, and added as the source terms to the momentum and energy equations respectively [10-11].

$$\vec{F}_L = \mathrm{Re}\left(\frac{1}{2}\vec{j}\times\widetilde{B}_{\theta\ Conjugate}\right). \tag{3}$$

$$Q = \mathrm{Re}\left(\frac{1}{2\sigma}\widetilde{\vec{j}}\times\widetilde{\vec{j}}_{\theta\ Conjugate}\right). \tag{4}$$

An enthalpy conservation equation is solved to model the solidification of the ingot:

$$\frac{\partial}{\partial t}(\rho h) + \nabla\cdot(\rho\vec{u}h) = \nabla\cdot(\lambda\nabla T) + Q + S. \tag{5}$$

Where λ is thermal conductivity of the alloy, and S is the source term of solidification latent heat. The treatment of solidification latent heat includes two parts:

$$S = -\frac{\partial}{\partial t}(\rho f L) - \rho L\vec{u}_s\nabla f \tag{6}$$

Eq. (6) ρ and L are density and latent heat of fusion, u_s is the casting velocity and f denotes the liquid fraction. The unsteady term in the right hand side of the Eq. (6) can be omitted when the process approaches steady state. We treat the steel as an effective binary Fe-C alloy system, and the alloy element C is very diffusive in both liquid and solid. Thus, lever rule [12] is chosen to calculate the liquid fraction as a function of temperature. The equation is expressed as:

$$f = \begin{cases} 1 & T > T_{liquidus} \\ 1-\left[(T_{liquidus}-T)/\left((T_f-T)(1-k_p)\right)\right] & T_{solidus} < T \le T_{liquidus} \\ 0 & T \le T_{solidus} \end{cases} \tag{7}$$

Where T_f is the melting point of solvent (1811 K) and k_p is the partition coefficient (k_p =0.35). The turbulence in the slag and liquid melt pool is modeled using SST-k-ω approach [13]. It is assumed that the turbulence kinetic energy is damping inside the mushy zone. For this purpose, a sink term for turbulence kinetic energy (k) is considered according to: $-10^6 k(1-f)$. Similarly, a sink term for the turbulence specific dissipation rate (ω) is used: $-10^6 \omega(1-f)$. It is beyond the scope of the present study to model the macrosegregation and solutal buoyancy driven flow. However, thermal buoyancy (Boussinesq approximation) and Lorentz force are taken into account as source terms for momentum equation. The drag resistance of the dendrites to the flow in the mushy region is estimated according to the permeability [14]. For the latter, the anisotropic model of Heinrich and Poirier is used [15].

$$K_{Parallel} = \begin{cases} 3.75\times10^{-4} f^2 d_1^2 & 0 < f \le 0.65 \\ 2.05\times10^{-7}\left[\dfrac{f}{1-f}\right]^{10.739} d_1^2 & 0.65 \le f \le 0.75 \\ 0.074\left(\ln(1-f)^{-1} - 1.49 + 2(1-f) - 0.5(1-f)^2\right) d_1^2 & 0.75 \le f < 1.0 \end{cases} \tag{8a}$$

$$K_{Perpendicular} = \begin{cases} 1.09\times10^{-3} f^{3.32} d_1^2 & 0 < f \le 0.65 \\ 4.04\times10^{-6}\left[\dfrac{f}{1-f}\right]^{6.7336} d_1^2 & 0.65 \le f \le 0.75 \\ \left[-6.49\times10^{-2} + 5.43\times10^{-2}\left[\dfrac{f}{1-f}\right]^{0.25}\right] d_1^2 & 0.75 \le f < 1.0 \end{cases} \tag{8b}$$

where d_1 refers to the spacing of the primary dendrite arm, $K_{Parallel}$ and $K_{Perpendicular}$ are the directional permeabilities. A number of models were presented to estimate the spacing of the dendrites arm according to the cooling rate and solute concentration [16]. Here, we used a model of Jacobi [17] where the size of the dendrites (expressed in μm) are computed according to the cooling rate, $\dot{T} = \vec{\nabla} T \cdot \vec{u}_s$, ahead of the crystallization front.

$$d_1 = 283\dot{T}^{-0.49} \tag{9}$$

The rate of cooling is considered to be very fast adjacent to the mold wall where the primary dendrite arm spacing is assumed constant (d_1 =50 μm). The heat radiation at air gap, slag-air, and ingot-air interfaces is considered using a value of 0.8 for the emissivity. The tip of the electrode takes the liquidus temperature of the steel. The free-slip boundary condition is applied for the flow at slag-pool interface, whereas the condition is no-slip at electrode-slag interface and at the mold wall. The boundary conditions for magnetic induction (Eq. 1) are obtained using ampere's law. In addition, the continuity of magnetic flux is applied at slag-pool, and electrode-slag interfaces [18].

The solidification of a conventional steel ingot (X12CrNiMoV) with the size (diameter: 750 mm, height: 1875 mm) was simulated. Diameter of the electrode is 500 mm. The industrial measurements of material properties of slag and steel that are temperature dependent are used for our simulations. Details about the operating conditions of the process and the average physical properties of the slag and alloy are described in Table 1. Transient calculation was made, but only the final steady state results are analyzed.

The simulation results were verified against experimental ingot (Fig. 2(c)). The pool profile was marked using solid tungsten granulate. The sizes of markers are in the range between 1 to 2 mm. Two lines are visible on the macrograph where the lower line is obtained by addition of tungsten to the process from a blind hole in the electrode. The upper line indicates the pool profile that was marked manually during remelting. Details about the conditions of the experiment were presented by Holzgruber [19].

Results and Discussions

The process is run under the frequency of 50 Hz and the electric current is allowed to cross the slag skin layer and flow through the mold as shown in Fig. 2(a). The skin effect, tendency of the electric current to flow near the surface, can be observed in the electrode, ingot, and mold.

The current re-enters to the steel ingot from the contact region (assumed to be 3 cm) between the solidified ingot and mold. Additionally, eddy currents generated in the copper mold can propagate

inside the steel ingot. As indicated in Fig. 2(b), the temperature is relatively uniform in the slag region due to rigorous stirring of the flow. The well-known flow recirculation under the edge of the electrode captures significant amount of heat released in the slag [18, 20]. Consequently, the hottest zone is under the shadow of the electrode where the flow is swirling. A relatively good agreement in the shape of melt pool is obtained between the simulation and experimental results, as shown in Fig. 2(c). Fig. 2(d) illustrates the distribution of primary dendrite arm spacing (PDAS). With the

Table 1. Averaged material properties and process parameters.

Slag	
Density (kg·m^{-3})	2650
Viscosity (kg·m^{-1}·s^{-1})	0.002
Specific heat, liquid (J·kg^{-1}·K^{-1})	1250
Thermal Conductivity, liquid (W·m^{-1}·K^{-1})	10
Electric Conductivity, liquid (ohm^{-1}·m^{-1})	120
Electric Conductivity, solid (ohm^{-1}·m^{-1})	15
Steel	
Density (kg·m^{-3})	7100
Viscosity (kg·m^{-1}·s^{-1})	0.006
Liquidus Temp. (K)	1760
Solidus Temp. (K)	1670
Thermal expan. Coefficient (K^{-1})	9x10^{-5}
Latent heat of fusion (J·kg^{-1})	260000
Thermal Conductivity, liquid(W·m^{-1}·K^{-1})	40
Electric Conductivity, liquid(ohm^{-1}·m^{-1})	8.8x10^{5}
Operating condition	
RMS current (kA)	14.1
AC frequency (Hz)	50
Slag height (m)	0.15

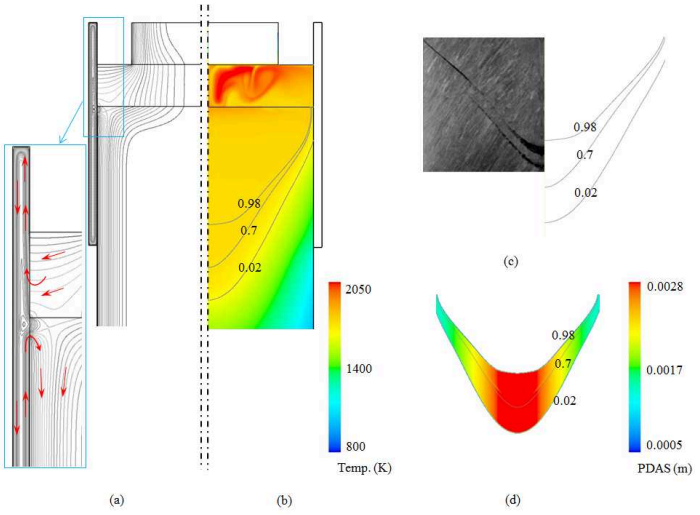

Fig. 2. (a) Electric current path (red arrows show the direction of electric current); (b) contour of temperature overlaid with isolines of fraction liquid (0.02, 0.7, 0.98) to indicate the mushy zone ; (c) Comparison of the experimental (left) with the numerical (right) results of the shape of the melt pool; (d) distribution of the calculated PDAS in the mushy zone.

increase of the distance from the mold wall toward the center, the cooling rate decreases and consequently the PDAS increase as well. As such, the largest PDAS (~ 2.8 mm) is observed in the region near to the ingot axis. The distribution of arm spacing is found to be dominantly parabolic inside the mushy zone. However, dendrites become finer with approximately uniform size in the vicinity of the ingot surface. The measuring data of dendritic structure is not available for this experimental ingot. Previously, Borodin [21] performed experiments on ESR ingots (ϕ 400 mm and ϕ 500 mm) of Cr-Mo-V to investigate crystal morphology and segregation of elements. The PDAS is observed to be in the range between 50 to 3000 μm which is not far from what we predicted by using Eq. (9). The influence of the interdendritic flow on the pool shape is studied by performing an additional simulation in which the PDAS is kept to be constant (d_1 =300 μm) inside the mushy zone. For the latter, it is observed that the V-shaped pool profile is relatively deep without flattening

at the center as shown in Fig. 3(a). However, flattening of the pool profile is predicted when the PDAS is computed using Eq. (9). In addition, the interdendritic melt flow is illustrated in Fig. 3(c). The relative velocity of interdendritic flow and casting velocity is zero for the case with constant arm space. Thus, the velocity of the melt inside the mushy zone is equal to the casting velocity. In contrast, the interdendritic flow is quite intensive for the case when the PDAS is computed using Eq. (9). It is found that melt can flow in any direction inside the mushy zone especially at large liquid fraction ($f > 0.7$).

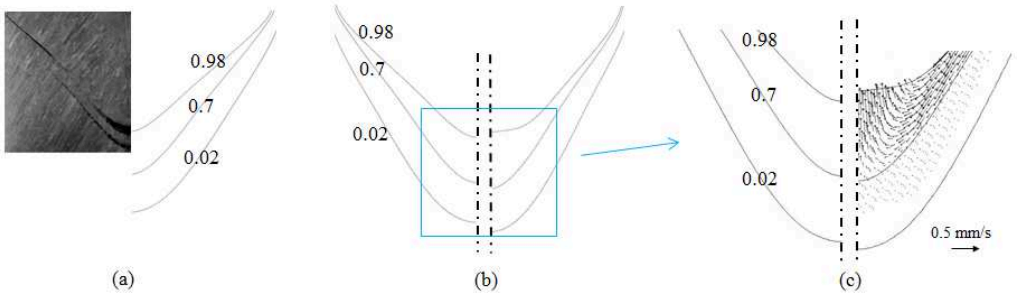

Fig. 3. (a) comparison of the experimental (left) result of the shape of the melt pool with the numerical (right) one when PDAS is assumed constant (d_1=300 μm); (b) shapes of melt pool predicted with a constant (left) PDAS vs. variable (right) PDAS; (c) interdendritic melt flow with a constant (left) PDAS vs. variable (right) PDAS.

Summary

A numerical study was performed to investigate the influence of crystal morphological parameters such as the primary dendrite arm spacing (PDAS) on the shape of the melt pool for an ESR ingot (ϕ 750 mm). The ESR process is operated under alternating electric current (50 Hz), and the electric current can cross the slag skin and enter into the mold. The shape of the melt pool was also measured experimentally in a plant trial. The distribution of PDAS is calculated as a function of the local cooling rate. Then, the computed PDAS is applied to estimate the directional permeability inside the mushy zone. Finally, the predicted pool profile is validated against the experiment. In addition, the effect of interdendritic flow is investigated by performing another simulation with an assumption of constant and homogenously distributed PDAS (d_1 = 300 μm) in the mushy zone. Different interdendritic melt flow and different shape of the melt pool were predicted in the two simulations. Essentially, the interdendritic flow is controlled by the permeability that strongly depends on the PDAS. Generally, the liquid velocity inside the mushy zone is significantly smaller than the velocity in the melt pool or slag. However, the two cases presented above were predicting different pool profile as a consequence of interdendritic velocity. For this reason, the permeability, PDAS, and interdendritic velocity must be modelled with extreme care to improve the accuracy of results.

Acknowledgements

The authors acknowledge the financial support by INTECO GmbH and the Austrian Federal Ministry of Economy, Family and Youth and the National Foundation for Research, Technology and Development within the framework of the Christian Doppler Laboratory for Advanced Process Simulation of Solidification and Melting.

References

[1] G. Hoyle, Electroslag Processes, Applied Science Publishers, London, 1983.

[2] E. Plöckinger, Electroslag remelting – A modern tool in metallurgy, J. of the Iron and Steel Institute, (1973) 533-541.

[3] K. O. Yu, J. A. Domingue, G.E. Maurer and H.D. Flanders, Macrosegregation in ESR and VAR processes, J. of Metals, (1986) 46-50.

[4] V. Weber, A. Jardy, B. Dussoubs, et al., A comprehensive model of the electroslag remelting process: description and validation, Metall. Trans. B, 40B (2009), 271-280.

[5] A.D Patel, M. Gierulal, D.J. Tallman, Bounds on model parameters for computational analysis of the ESR process, Proc. of LMPC, USA (2009), 201-211.

[6] M.J.M. Krane, M. Fahrmann, Jeff Yanke, et al., A comparison of predictions of transport phenomena in electroslag remelting to industrial data, Proc. of LMPC, France (2011), 65-72.

[7] P.C. Carman, Flow of gases through porous media, Butterworths Publisher, London, 1956.

[8] W. Schutzenhofer, G.Reiter, R. Tanzer, et al., Experimental investigations for the validation of a numerical PESR-model, Proc. of LMPC, France (2007), 49-54.

[9] Z. Jiang and Y. Dong, Solidification model for electroslag remelting process, Proc. of LMPC, France (2007), 89-94.

[10] A. Kharicha, M. Wu, A. Ludwig, B. Ofner, H. Holzgruber, CFD Modeling and simulation in materials processing, Wiley publication, USA, 2012, pp. 139-148.

[11] A. Kharicha, W. Schützenhöfer, A. Ludwig and R. Tanzer, Numerical and experimental investigations on the ESR process of the hot work tool steel H11, Proc. of LMPC, USA (2009) 235-242.

[12] T.W. Clyne, W. Kurz, Solute redistribution during solidification with rapid solid state diffusion, Metall. Trans., 12A (1981), 965-971.

[13] F. R. Menter, Two-equation eddy-Viscosity turbulence models for engineering applications, AIAA Journal, 32 (8) (1994) 1598-1605.

[14] M. C. Schneider and C. Beckermann, A numerical study of the combined effects of micro segregation, mushy zone permeability and flow, caused by volume contraction and thermosolutal convection, on macrosegregation and eutectic formation in binary alloy solidification, Int. J. Heat Mass Transfer, 38(18) (1995) 3455-3473.

[15] J. C. Heinrich and D. R. Poirier, Convection modeling in directional solidification, Comptes Rendus Mecanique, 332 (5-6) (2004), 429-445.

[16] E. J. Pickering, Macrosegregation in steel ingots: the applicability of modeling and characterization techniques, ISIJ Int., 53 (6) (2013) 935-949.

[17] H. Jacobi and K. Schwerdtfeger, Dendritic morphology of steady state unidirectionally solidified steel, Metall. Trans. A, 7A (1976) 811-819.

[18] E. Karimi Sibaki, A. Kharicha, M. Wu, A. Ludwig, H. Holzgruber, B. Ofner, M. Ramprecht, A numerical study on the influence of the frequency of the applied AC current on the electroslag remelting process, Proc. of LMPC, USA (2013), 13-19.

[19] H. Holzgruber, W. Holzgruber, A. Scheriau, et al, Investigation of the implications of the current conductive mold technology with respect to the internal and surface quality of ESR ingots, Proc. of LMPC, France (2011) 57-64.

[20] A. H. Dilawari, and J. Szekely, Heat transfer and fluid flow phenomena in electroslag refining, Metall. Trans. B, 9B (1975) 77-87.

[21] I. P. Borodin, V. A. Goryainov, V. S. Koshman, et al., Influence of solidification conditions on dendritic structure and segregation of elements in electroslag remelted ingots, Steel in the USSR (15) (1985) 533-537.